JACS
JOURNAL OF THE AMERICAN CHEMICAL SOCIETY
Article
pubs.acs.org/JACS

Interplay between Mechanical, Electrical, and Thermal Relaxations in Nanocomposite Proton Conducting Membranes Based on Nafion and a $[(ZrO_2)\cdot(Ta_2O_5)_{0.119}]$ Core–Shell Nanofiller

Vito Di Noto,*[,†] Matteo Piga,[†] Guinevere A. Giffin,[†] Keti Vezzù,[†,§] and Thomas A. Zawodzinski[‡]

[†] Department of Chemical Sciences, University of Padova, Via Marzolo 1, I-35131, Padova (PD), Italy

[‡] Department of Chemical and Biomolecular Engineering, University of Tennessee, 442 Dougherty Engineering Building, Knoxville, Tennessee 37996-2200, United States

ABSTRACT: The thermal, mechanical, and electric properties of hybrid membranes based on Nafion that contain a $[(ZrO_2)\cdot(Ta_2O_5)_{0.119}]$ "core–shell" nanofiller are elucidated. DSC investigations reveal the presence of four endothermic transitions between 50 and 300 °C. The DMA results indicate improved mechanical stability of the hybrid materials. The DSC and DMA results are consistent with our previous suggestion of dynamic $R-SO_3H\cdots[ZrTa]$ cross-links in the material. These increase the thermal stability of the $-SO_3H$ groups and the temperature of thermal relaxation events occurring in hydrophobic domains of Nafion. The broadband electrical spectroscopic analysis reveals two electric relaxations associated with the material's interfacial (σ_{IP}) and bulk proton conductivities (σ_{EP}). The wet $[Nafion/(ZrTa)_{1.042}]$ membrane has a conductivity of 7.0×10^{-2} S cm^{-1} at 115 °C, while Nafion has a conductivity of 3.3×10^{-2} S cm^{-1} at the same temperature and humidification conditions. σ_{EP} shows VTF behavior, suggesting that the long-range conductivity is closely related to the segmental motion of the Nafion host matrix. Long-range conduction (σ_{EP}) occurs when the dynamics of the fluorocarbon matrix induces contact between different delocalization bodies (DB), which results in proton exchange processes between these DBs.

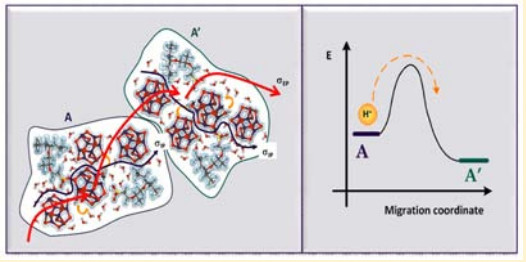

1. INTRODUCTION

Fuel cells are used to convert the chemical energy of the fuel into electrical energy and have several advantages over conventional energy conversion devices. As compared to the internal combustion engine, fuel cells have increased energy conversion efficiency, reduced oil consumption, increased fuel flexibility, and reduced CO_2 and pollutant emissions.[1,2] Proton exchange membrane fuel cells (PEMFCs) are of particular interest because they are compact, lightweight, and have high power densities with high current densities as compared to some of the other families of fuel cells.[3] At the heart of the PEMFC is the proton exchange membrane (PEM). A good PEM exhibits high chemical, electrochemical, and thermal stability, low reactant permeability, high proton conductivity, and low production costs.[4,5] Despite many years of research, Nafion and similar perfluorosulfonic acid (PFSA) membranes remain the standard membrane of reference. There are however several drawbacks to using Nafion or virtually any other PEM described to date, such as low conductivity at temperatures above 90 °C and low levels of relative humidity, high price, and environmental issues associated with the synthesis and disposal of perfluorinated membranes.[6,7] As a result, significant research has been focused on alternatives to Nafion. According to the U.S. Department of Energy, new membranes should exhibit a low areal specific resistance (0.02 ohm cm^2) at the targeted operating conditions of high temperature (120 °C) and low relative humidity (40–80 kPa P_{water}), and the cost must be reduced to 20 USD/m^2.[1]

One promising research avenue is focused on the preparation of organic–inorganic composite membranes based on Nafion and inorganic fillers in the micrometer to nanometer size range.[8−15] Nafion membranes doped with heteropolyacids, such as phosphotungstic acid (PTA), permit improved performance at lower relative humidities and elevated temperature (ca. 120 °C), while hygroscopic oxides, such as SiO_2, TiO_2, ZrO_2, Al_2O_3, and others, increase the water uptake of the membranes and decrease the humidification requirements of the PEMFCs.[8−15] Recently, membranes that incorporate $[(M1_mO_n)\cdot(M2_xO_y)_z]$ "core–shell" nanofillers have shown improved mechanical properties and proton conductivities when compared to Nafion and $[Nafion/(M_xO_y)_n]$ membranes.[16−18] The nanofiller is prepared by milling two oxides with different Mohs indices and acidity together in the presence of a solvent to produce nanometric particles consisting of a "core" of the harder oxide ($M1_mO_n$) covered by a thin layer of the softer oxide ($M2_xO_y$).[16−19]

This Article describes studies on new proton conducting membranes based on Nafion and a $[(ZrO_2)\cdot(Ta_2O_5)_{0.119}]$ nanofiller (ZrTa). It was demonstrated elsewhere[20] that ZrTa has a "core–shell" morphology, where the harder ZrO_2 forms the "core" and is covered by a "shell" of the softer Ta_2O_5. ZrTa is a Type A "core–shell" filler, where there is a chemical interaction between the two oxides.[20] The hybrid membranes

Received: July 26, 2012
Published: October 26, 2012

dx.doi.org/10.1021/ja3071336 | J. Am. Chem. Soc. 2012, 134, 19099–19107

have a reduced water uptake and are thermally stable up to 170 °C.[20] Fuel cell tests in single cell configuration show that membrane electrode assemblies containing the hybrid membrane have higher power densities than Nafion particularly at low values of relative humidity.[20] The focus of this work is the relationship between the structure and relaxations of the hybrid membranes. The membranes are characterized with differential scanning calorimetry, dynamic mechanical analysis, and broadband electrical spectroscopy (BES). These results are correlated with structural characterization described elsewhere[20] to elucidate further the structure−relaxation relationships occurring within these hybrid materials. In particular, the stabilizing effect of the filler on the dynamics of the hydrophobic and hydrophilic domains of the membranes through the formation of dynamic R−SO_3H···[ZrTa]···HO_3S−R cross-links is investigated. These cross-linking interactions contribute to the development of a hybrid three-dimensional network that binds the fluorocarbon chains of Nafion and regulates the long-range charge transfer mechanism.

2. EXPERIMENTAL SECTION

2.1. Nanofiller and Membrane Preparation. The ZrTa nanofiller and membranes were prepared as described elsewhere,[20] and their preparation is only briefly summarized here. A dimethylformamide suspension containing ZrO_2 (Aldrich, ACS grade) and Ta_2O_5 (Aldrich, ACS grade) was milled for 5 h at 500 rpm in a tungsten carbide grinding jar using a planetary ball mill (RETSCH PM 100). The mixture was diluted with DMF and treated in an ultrasonic bath for 1 h. This suspension contained the "core−shell" ZrTa nanoparticles. [Nafion/$(ZrTa)_\Psi$] nanocomposite membranes with Ψ = 0, 0.316, 0.542, 1.042, 1.316, 1.610, and 1.926 where $\Psi = (mol_{ZrO_2} + mol_{Ta_2O_5})/mol_{-SO_3H}$ were prepared using a general solvent casting procedure. Nafion (5 wt % perfluorosulfonic acid PTFE copolymer solution, Alfa Aesar, ACS grade) suspended in a water/alcohol mixture was cast to remove the low-boiling solvents. The resulting brittle film was dissolved in DMF and mixed with an appropriate amount of the nanofiller suspension.[16,17] The mixture was homogenized in ultrasonic bath for 2 h and was then recast on a Petri dish. The membrane was dried under air at room temperature for 1 h, placed in oven at 130 °C for 4 h, and hot-pressed at 100 °C and 68 bar for 5 min. The thickness of the films was between 200 and 280 μm. The hybrid membranes were purified and activated by a series of treatments at 80 °C as described in detail elsewhere.[16] Each membrane was soaked in double-distilled water, a 3 wt % solution of H_2O_2, a 1 M H_2SO_4 solution, and three times in double-distilled water for 1 h. After this treatment, the films were hydrated in an autoclave at 100% relative humidity, 135 °C, and 3.3 bar. This hydrated state was considered the "reference zero point" (RZP) of the membranes thermal history. The membranes were stored in PET bags filled with double-distilled water at room temperature. The electrical measurements were conducted in the RZP conditions, while the samples for the thermal and mechanical measurements were dried under air for 60 min. Drying in these conditions results in membranes that are easy to manipulate and are representative of all of the interactions present in multiphasic hybrid Nafion membranes; the water content is between λ = 0.2 and 1.1.[20] The water uptake of the [Nafion/$(ZrTa)_\Psi$] membranes is λ = 12.5 at Ψ = 0.316, λ = 9.1 at Ψ = 0.542, λ = 10.9 at Ψ = 1.042, λ = 13.1 at Ψ = 1.316, λ = 10.6 at Ψ = 1.61, and λ = 13.2 at Ψ = 1.926.[20]

2.2. Instruments and Methods. Differential scanning calorimetry (DSC) measurements were carried out with a DSC 2920 differential scanning calorimeter (TA Instruments) equipped with a LNCA low-temperature attachment operating under a helium flux of 30 cm^3 min^{-1}. Measurements are performed with a heating rate of 3 °C min^{-1} between −50 and 300 °C on about 4 mg of sample sealed in an aluminum pan. Dynamic mechanical analyses (DMA) were carried out with a TA Instruments DMA Q800 instrument equipped a film/fiber tension clamp. The spectra were collected between −10 and 200 °C with a heating rate of 4 °C min^{-1} by subjecting a rectangular film with dimensions of ca. 25 (height) × 6 (width) × 0.2 (thickness) mm to an oscillatory sinusoidal tensile deformation with an amplitude of 4 μm at 1 Hz and a 0.05 N preloading force.

The complex impedance spectra of membranes in the RZP state were measured in the frequency range from 10 mHz to 10 MHz and temperature range from 5 to 155 °C using a Novocontrol Alpha-A analyzer. The temperature was increased in 10 °C increments using a homemade cryostat operating with a N_2 gas jet heating and cooling system. The temperature was measured with an accuracy higher than ±0.4 °C. The freshly autoclaved membrane was sandwiched between two circular platinum electrodes and placed in a closed homemade Teflon cell. The free volume of the cell was partially filled with 100 μL of double-distilled water to avoid drying during measurements up to 155 °C. The geometrical cell constant was determined by measuring the electrode−electrolyte contact surface and the distance between the electrodes. No corrections for the thermal expansion of the cell were used. The complex impedance ($Z^*(\omega) = Z'(\omega) + iZ''(\omega)$) was converted into complex conductivity ($\sigma^*(\omega) = \sigma'(\omega) + i\sigma''(\omega)$) and complex permittivity ($\varepsilon^*(\omega) = \varepsilon'(\omega) - i\varepsilon''(\omega)$) using the equations $\sigma^*(\omega) = k[Z^*(\omega)]^{-1}$ and $\sigma^*(\omega) = i\omega\varepsilon_o\varepsilon^*\omega$, respectively, where k is the cell constant and $\omega = 2\pi f$ (f is the frequency in Hz).

3. RESULTS AND DISCUSSION

The correlation between the structure and the thermal, mechanical, and electrical relaxations is of use to define the effect of the Nafion−filler interactions on the thermal and mechanical properties and the conductivity mechanism of the hybrid membranes.

3.1. Thermal Transitions. DSC is a useful technique to examine the thermal transitions of materials. These transitions often play an important role in the mechanical and electric properties of a material. The DSC curves of the [Nafion/$(ZrTa)_\Psi$] membranes, reported in Figure 1, reveal the presence of four overlapping endothermic peaks: I, II, III, and IV. The observed DSC curves are well described by a series of Gaussian

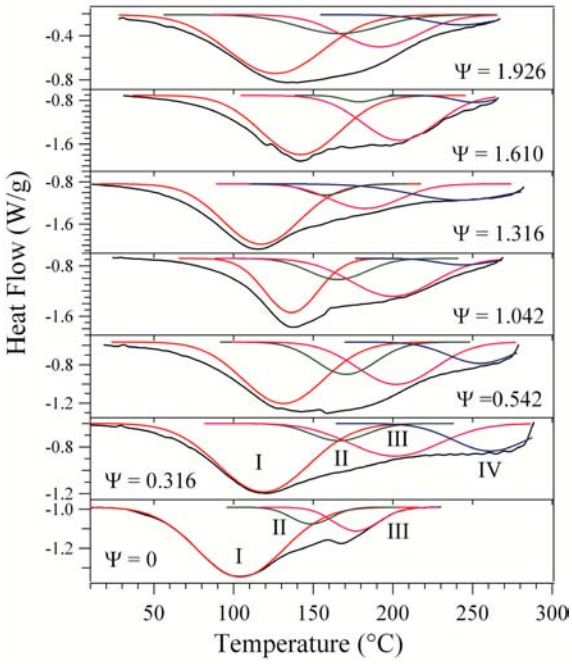

Figure 1. DSC curves [Nafion/$(ZrTa)_\Psi$] membranes. Ψ signifies the nanofiller concentration. The DSC curves are decomposed with Gaussian functions in the 40−280 °C temperature range. I−IV indicate the detected endothermic peaks.

dx.doi.org/10.1021/ja3071336 | J. Am. Chem. Soc. 2012, 134, 19099−19107

peaks. This approach is accepted for discerning overlapping peaks contributing to a complex experimental profile. The temperatures of peak positions, reported in Table 1, depend on the nanofiller concentration and were determined by fitting the DSC experimental curves with Gaussian functions.[16]

Table 1. DSC Transition Temperatures of the [Nafion/(ZrTa)$_\Psi$] Membranes

Ψ	peak I/°C	peak II/°C	peak III/°C	peak IV/°C
0.000	104	149	177	
0.316	119	166	201	261
0.542	131	171	202	255
1.042	136	165	200	244
1.316	117	157	182	243
1.610	142	179	204	251
1.926	126	166	192	243

Peak I is assigned to the melting of small and imperfect fluorocarbon nanocrystalline domains of Nafion.[16,21] A similar peak is also present in other PEMs, such as sulfonated polyetheretherketone,[22,23] and arises from the coexistence of a partially crystalline polymer matrix and polar domains. The presence of the hydrogen-bonding interactions between the acid groups in the polar domains reduces the size of the ordered microdomains of the polymer matrix, which generates the nanocrystalline domains.[18,19] The temperature of peak I, reported in Table 1, is higher for the hybrid membranes than Nafion, which suggests that hydrophobic nanodomains are stabilized by the dipolar nanofiller−Nafion cross-links (R−SO_3H···[ZrTa]) present in hydrophilic regions.[20] Therefore, thermal event I, which reflects the type and strength of side group−environment interactions within the Nafion host polymer, indicates that the size of the hydrophobic PTFE domains of the Nafion host matrix increases due to the interaction with the nanofiller. Peak II (140−220 °C) is assigned to the endothermic degradation of acid −SO_3H groups in accordance with thermogravimetric analysis, as discussed elsewhere.[20] The increased decomposition temperature of the acid groups in the hybrid membranes indicates that the strong dynamic RSO_3H···[ZrTa] interactions act to thermally stabilize the SO_3H groups.

Peaks III (170−205 °C) and IV (240−270 °C) are attributed to the melting transitions of the hydrophobic fluorocarbon microcrystalline regions in Nafion with increasing size (III < IV).[16] Peaks III and IV in the [Nafion/(ZrTa)$_\Psi$] membranes are found at temperatures higher than those in pristine Nafion, which is in agreement with the observations made with respect to peak I.

From these results, it is inferred that the PTFE domains of the Nafion matrix have increased in size in the hybrid membranes.

3.2. Dynamic-Mechanical Analysis. The mechanical properties have been highlighted[24] and are only briefly summarized here. The storage modulus at Ψ > 0.316 is higher than Nafion and increases with increasing Ψ.[24] Nafion experiences an irreversible elongation above 160 °C, but this elongation does not occur in the hybrid membranes. The storage modulus of the hybrid membranes, for Ψ > 0.542, remains above 1 MPa up to 200 °C.[24] The high storage modulus even at high temperatures and the lack of an irreversible elongation in the hybrid membranes are consistent with the idea that a density of dynamic R−SO_3H···[ZrTa] cross-links occurs within the [Nafion/(ZrTa)$_\Psi$] membranes. The density of dynamic cross-links is also responsible for the reduced water uptake of hybrid materials.[20] Increasing the number of dynamic cross-links decreases the W.U., which suggests that when R−SO_3H side groups are involved in R−SO_3H···[ZrTa] interactions, the free volume of the hybrid membranes decreases, and a smaller quantity of bulk water clusters is absorbed by the voids present in the hydrophilic domains of the hybrid membranes. Also, the modulus increases, making the polymers more difficult to swell.

The incorporation of inorganic fillers does not always result in an improvement of the mechanical properties of hybrid membranes. This suggests that the interaction of the filler with the host matrix, and therefore the chemical composition of the incorporated filler, plays an important role in the mechanical properties. Studies on silica-based hybrid membranes showed that the mechanical properties varied with the amount of filler. At low concentrations (3 wt %), the silica improves the elastic modulus, but as the wt % increases, the elastic modulus and Young's modulus decrease.[25,26] It has been suggested that high concentrations of silica (5 wt % and higher) results in the formation a rigid scaffold within the membrane and increases the membranes' brittleness.[26] Silica does not strongly interact with the host matrix, so small amounts can provide mechanical strength to the matrix, but larger amounts disrupt the dynamic cross-links between the side group moieties that provide the mechanical stability in the pristine matrix. In contrast, the mechanical properties increase with the amount of filler added up to 21 wt % in the [Nafion/(ZrTa)$_\Psi$] membranes. When various metal oxides are used as dopants, the mechanical properties of the composite membranes are found to depend on the identity and the chemical properties of the metal oxide. In a series of metal oxide-containing membranes: (a) the temperature of the mechanical tan δ peak shifted with the identity of the metal oxide;[10] and (b) the best mechanical properties occurred in the HfO_2-containing membrane.[27] Strong acid−base interactions occur between the basic HfO_2 and the sulfonic acid groups of host polymer matrix in the hydrophilic domains. A comparison of the mechanical results of the [Nafion/(ZrTa)$_\Psi$] membranes with those of the [Nafion/$(M_xO_y)_n$] membranes reveals that the interactions occurring between the metal oxide and matrix have a direct effect on the mechanical properties of the membrane. The steady improvement of the mechanical properties of the [Nafion/(ZrTa)$_\Psi$] membranes with increasing filler concentration supports the interpretation that there is a strong interaction between the nanofiller and the Nafion matrix.

The influence of the Nafion−nanofiller interactions on the mechanical relaxations of the membranes is investigated by analyzing tan $\delta = E''/E'$ profiles reported in Figure 2. These curves reveal the presence of four mechanical relaxation events, α_{pc}, α_{pc}', α, and α'.[16] The α_{pc} and α_{pc}' modes are assigned to the long-range motion of both the backbone and the side chains facilitated by the weakening of the electrostatic interactions within the ionic aggregates.[16,21,24] The α_{pc}' relaxation occurs within the hydrophobic PTFE-like domains, which, as argued above, increase in size due to the Nafion−nanofiller interactions, while α_{pc} corresponds to the PTFE-like domains with sizes smaller than those in Nafion.[16]

The α and α' relaxation events, measured around 40 and 65 °C, are attributed to the $13_6 \rightarrow 15_7$ helix transformation and to the order−disorder conformational transitions occurring in hydrophobic PTFE-like domains of Nafion, respectively.[16,17]

dx.doi.org/10.1021/ja3071336 | J. Am. Chem. Soc. 2012, 134, 19099−19107

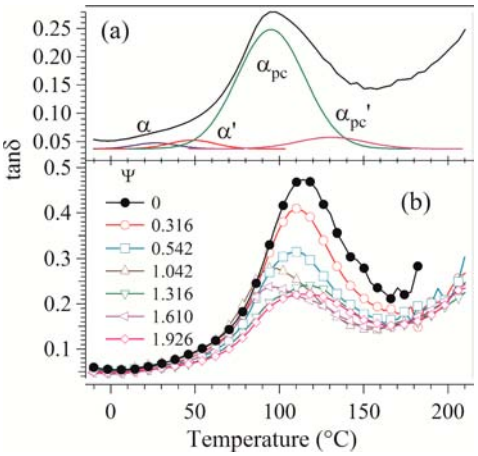

Figure 2. (a) tan δ as a function of temperature of the [Nafion/(ZrTa)$_\Psi$] membranes. (b) Typical fit of α_{pc}, α_{pc}', α, and α' relaxation modes.

These assignments are based on the works of Zerbi et al.[28,29] and Clark,[30] who reported the presence of such transitions in PTFE at 19 and 30 °C. The transition at 19 °C is associated with a conformational transition between the 13_6 and 15_7 helical geometries of the PTFE chains, while the transition at 30 °C is due to the partial destruction of the crystalline order along the chains.[28,29] Therefore, the α and α' mechanical transitions are associated with the dynamics of the PTFE chains of Nafion. The mechanical transition temperatures were determined by fitting the tan δ profiles with Gaussian functions,[16] as shown in Figure 2a. The values of both T_α and $T_{\alpha'}$ in the hybrid membranes are lower than those in pristine Nafion, which suggests that the oxoclusters facilitate the mechanical chain mobility (PTFE segmental motion) due to the dynamic R−SO_3H···[ZrTa] interactions in polar ionic aggregate domains .

3.3. Broadband Electrical Spectroscopy. The electrical properties of the [Nafion/(ZrTa)$_\Psi$] membranes in RZP conditions are investigated by BES. The three-dimensional surfaces of the imaginary component of the permittivity ε'' and the real part of the conductivity σ' for pristine Nafion and the hybrid membrane with Ψ = 1.610 are reported as a function of temperature and frequency in Figure 3.

The spectra of ε'' show (a) a peak at frequencies greater than 10^5 Hz, which shifts to higher frequencies with increasing temperature and corresponds to a rapid increase followed by a

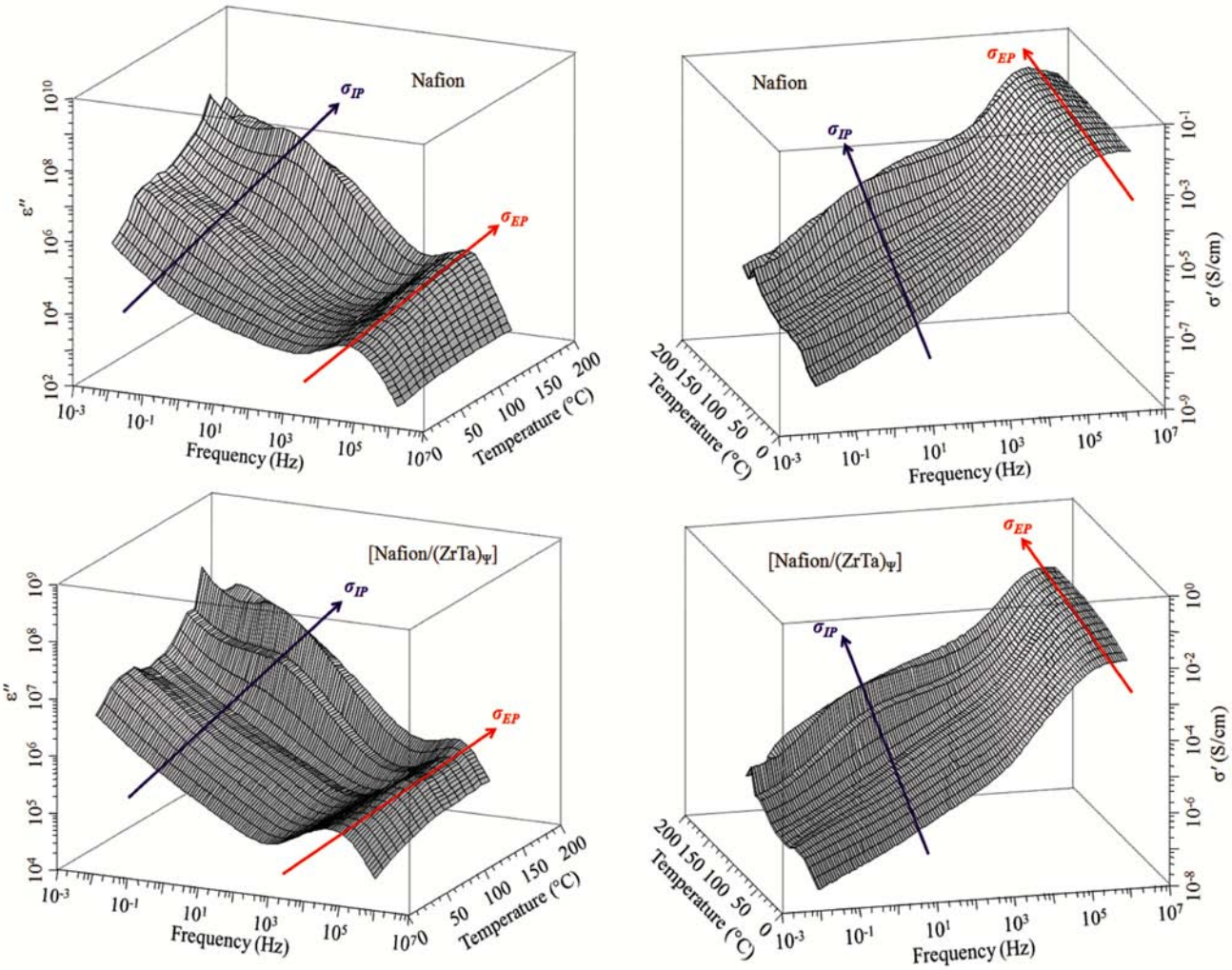

Figure 3. 3D surface of the imaginary component of the permittivity and the real component of the conductivity as a function of temperature and frequency for Nafion and the [Nafion/(ZrTa)$_\Psi$] membrane with Ψ = 1.61.

dx.doi.org/10.1021/ja3071336 | J. Am. Chem. Soc. 2012, 134, 19099−19107

plateau in σ'; and (b) a second event at frequencies less than 10^3 Hz that increases with increasing temperature, identified by increasing values of ε'' with decreasing frequency, and corresponds to the appearance of a second plateau in the σ' profiles. The σ' values taken from the high-frequency plateau correspond to the "bulk" conductivity of the materials.[16,17] The presence of the intense peak in ε'' and the corresponding decrease of σ' is due to the electrode polarization (EP) phenomenon, which is caused by the measuring electrodes that block the charge carriers at the interface between the electrodes and the polymeric membranes. The values associated with this phenomenon correspond to the "bulk" conductivity, σ_{EP}.[31] The electrical event present at medium frequencies is due to interfacial polarization (IP) associated with the conductivity σ_{IP}. The presence of the secondary conductivity contributions at high temperatures is typically observed in ionic conductors consisting of two or more phases, which have different dielectric constants,[31] and results from the accumulation of charge at the interfaces between these phases. In Nafion, the conductivity σ_{IP} results from the coexistence of the hydrophobic domains containing the PTFE-like matrix with low permittivity ($\varepsilon' \approx 2.2$)[32] and the polar conducting domains, which consist of the acid groups and water molecules with higher permittivity ($\varepsilon' \approx 78$).[33]

The electric relaxations associated with the electrode (σ_{EP}) and interfacial (σ_{IP}) conductivities are easily observable in the tan $\delta = \varepsilon''/\varepsilon'$ profiles in Figure 4. The tan δ profiles clearly show the presence of two peaks that shift to higher frequencies with increasing temperature. As in the σ' and ε'' spectra, the first peak at frequencies lower than 10^3 Hz is due to the interfacial conductivity σ_{IP}, while the second more intense event at frequencies above 10^4 Hz is associated with the "bulk" conductivity σ_{EP}. To determine the values of the conductivity and the relaxation times associated with the EP and IP polarization phenomena, the experimental profiles are analyzed with eq 1.[18,23]

$$\varepsilon^* = \sum_{k=1}^{2} \frac{\sigma_k}{i\omega\varepsilon_0} \frac{(i\omega\tau_k)^{\gamma_k}}{[1 + (i\omega\tau_k)^{\gamma_k}]} + \varepsilon_\infty \quad (1)$$

This equation accounts for the electrode ($k = 1$) and interfacial ($k = 2$) polarization phenomena. σ_k and τ_k are the conductivity and relaxation time associated with the kth polarization, while γ_k is a shape parameter that describes the broadness and asymmetry of the kth peak.[31] Equation 1 is used to simultaneously fit the spectra of ε', ε'', σ', and σ'' based on the relationship between the complex conductivity and the complex permittivity, $\sigma^* = i\omega\varepsilon_0\varepsilon^*$. An example of the fitting results, where the experimental curves of ε'' and σ' are decomposed into the EP (related to σ_{EP} and f_{EP}) and IP (associated with σ_{IP} and f_{IP}) components, is reported in Figure 5.

The profiles of $\sigma'(\omega)$, which correspond to the electrode polarization, are typically present in polymer electrolytes and can be simulated with an equivalent circuit, that is, combining resistors and capacitors in series and parallel.[31] The electrode polarization phenomenon can be modeled with a resistor and two capacitors in series.[23] The resistor R simulates the "bulk" conductivity, while the capacitors C_{EP} simulate the accumulation of charge at the two interfaces between the sample and the blocking electrodes. If $d_{EP}/2$ is the thickness of each interfacial region near the electrodes and L is the total sample length, for $L \gg d_{EP}$ it is possible to obtain the total complex permittivity ε^* and the relaxation time τ_{EP} associated with the EP using the following expressions:[23]

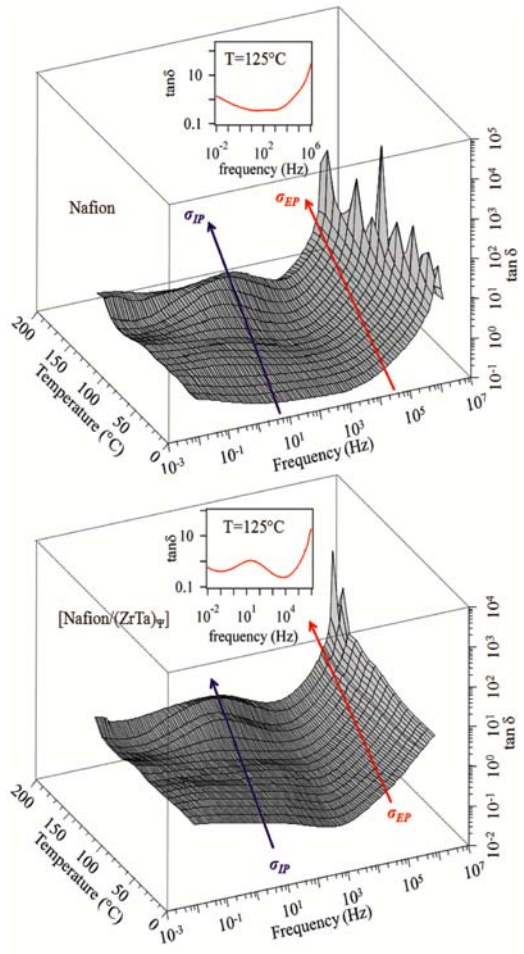

Figure 4. 3D surface of tan δ as a function of temperature and frequency for Nafion and the [Nafion/(ZrTa)$_\Psi$] membrane with Ψ = 1.61. The insets show the 2D tan δ profile at T = 125 °C.

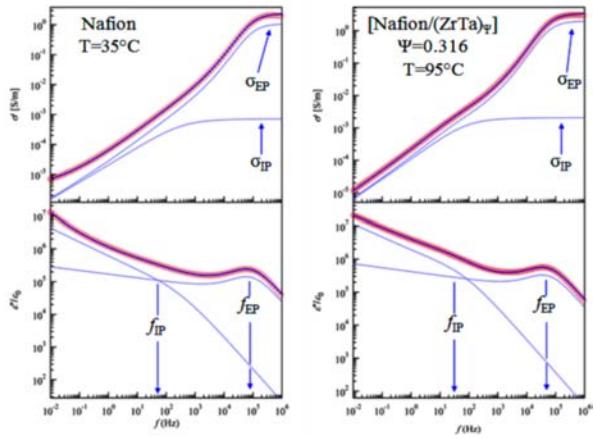

Figure 5. Fit of ε'' and σ' for (a) pristine Nafion and (b) the [Nafion/(ZrTa)$_\Psi$] membrane with Ψ = 0.316. σ_{EP}, f_{EP} and σ_{IP}, f_{IP} are the conductivity and the relaxation frequencies related to the electrode and interfacial polarizations, respectively. The circles are the experimental data points, the thick line is the fit curve, and the thin lines are the component curves.

dx.doi.org/10.1021/ja3071336 | J. Am. Chem. Soc. 2012, 134, 19099−19107

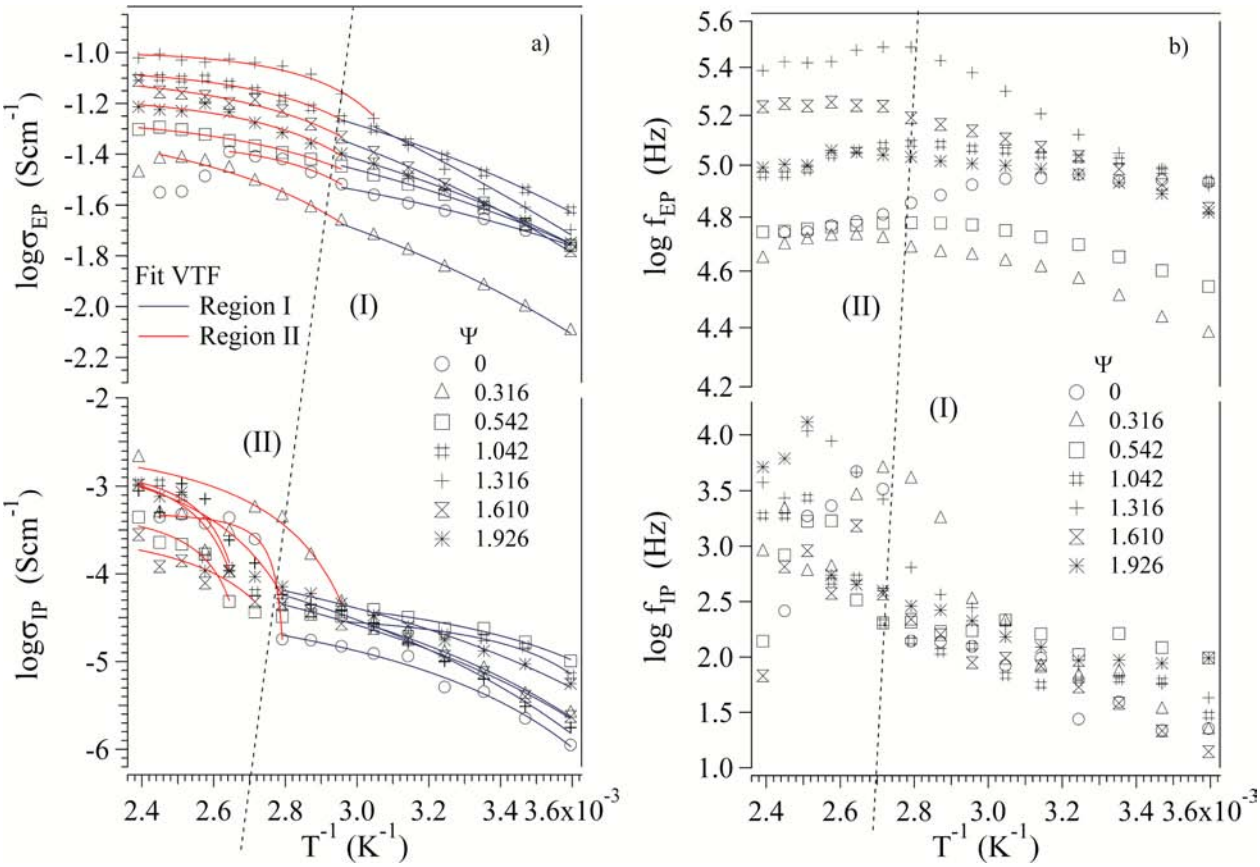

Figure 6. (a) Bulk (σ_{EP}) and interfacial (σ_{IP}) conductivities as a function of T^{-1}. (b) Frequencies f_{EP} and f_{IP} associated with the bulk and interfacial conductivities. I and II indicate the different temperature regions where the data are fitted with the VTF (solid line) equation. The σ_{EP} data have been previously demonstrated[24] and are shown here for comparison.

$$\varepsilon^* = \frac{\sigma_{EP}}{i\omega\varepsilon_0}\frac{(i\omega\tau_{EP})^{\gamma_{EP}}}{[1 + (i\omega\tau_{EP})^{\gamma_{EP}}]} + \varepsilon_\infty \quad (2)$$

$$\tau_{EP} = \frac{\varepsilon_0\varepsilon_{EP}}{\sigma_{EP}}\left(\frac{L - d_{EP}}{d_{EP}}\right) \quad (3)$$

In eqs 2 and 3, σ_{EP} is the bulk conductivity and ε_{EP} is the complex permittivity of the interfacial region. ε_o and ε_∞ are the vacuum permittivity and the electronic contribution to the material permittivity, respectively. Typically d_{EP} is on the order of nanometers,[34] while the thickness L of these materials is about 200 μm, so the condition $L \gg d_{EP}$ is satisfied. Equation 3 indicates that τ_{EP} increases with the sample thickness L and decreases with increasing charge carrier concentration and mobility. For the [Nafion/(ZrTa)$_\Psi$] membranes, eq 3 can be used to analyze the relaxation time $\tau_{EP} = 1/f_{EP}$ and the conductivity σ_{EP}, which are read directly from the high frequency peak position in the ε'' spectra and the conductivity plateau in the σ' spectra, respectively.

According to eq 3, considering that the electrode area and the sample length L are constant and assuming that $d_{EP} \approx 1$ nm is almost constant for all of the membranes,[35] an increase in the σ_{EP} conductivity should lead to a reduction of τ_{EP}. This is generally true between 5 and ca. 95 °C. Above ca. 95 °C, both the conductivity and the relaxation time increase. From eq 2, this is possible if there is an increase in the permittivity ε_{EP} of the interfacial region. Changes in ε_{EP} at high temperatures may be related to the α_{pc} relaxation above 85 °C in Nafion and above ca. 100 °C in the hybrid membranes that involves a weakening of the interactions within the polar domains.

The values of the conductivities σ_{EP} and σ_{IP}, obtained by fitting the experimental data with eq 1, are reported as a function of reciprocal temperature in Figure 6a. The conductivities σ_{EP} have been previously highlighted,[24] but discussed here in detail. The temperature dependence of log σ_{EP} and log σ_{IP} can be divided into two different temperature regions, I (below 75 °C) and II (above 75 °C). Except for the membrane with Ψ = 0.316, the bulk conductivity σ_{EP} of the hybrid membranes is higher than that of pristine Nafion. The highest value of conductivity is observed for the nanocomposite membrane with Ψ = 1.316, which exhibits σ_{EP} values of 7.5 × 10^{-2} at 115 °C and 7.7 × 10^{-2} S cm^{-1} at 135 °C at RZP conditions.

The conductivities σ_{EP} and σ_{IP} show the typical Vogel–Tamman–Fulcher (VTF) behavior,[16,25,36] which indicates that segmental motion of the polymer host is a crucial factor in the modulation of the charge transfer mechanisms. The interfacial conductivity σ_{IP} is 2–3 orders of magnitude lower than σ_{EP}. In region I, σ_{IP} is higher in the hybrid membranes than in Nafion. This evidence suggests that the ZrTa nanofiller enhances the charge accumulation at the interfaces between the hydrophobic and hydrophilic domains. Also, the protons are delocalized at the Nafion–nanofiller interfaces in the presence of water.

As discussed above, there is a decoupling of σ_{EP} and τ_{EP} above 95 °C (Figure 6). This effect results from a change in the conductivity behavior, which occurs between the temperature regions I and II. According to the DMA analysis, the hybrid

dx.doi.org/10.1021/ja3071336 | J. Am. Chem. Soc. 2012, 134, 19099–19107

materials undergo the α_{pc} mechanical transition above ca. 100 °C. This transition, in addition to a weakening of the electrostatic interactions, implies a weakening of the dipolar interactions and thereby an increase in the motion of both the primary and the secondary structures of Nafion. Therefore, it is reasonable to hypothesize that this relaxation alters the structure of the membrane and the interfacial layer between the membrane and the blocking electrodes, resulting in an increase in its permittivity ε_{EP}. This interpretation is in agreement with DSC results that show a broad endothermic peak around 100 °C, with an onset temperature around 70 °C, mainly due to the melting of the semicrystalline PTFE-like nanodomains of Nafion. It is also possible to hypothesize that above 80 °C there is an increase in the amorphous fraction of the membranes that yields a more homogeneous distribution of the hydrophilic domains within the hydrophobic polymer matrix. This structural reorganization increases the polar character of the membrane and thus its dielectric permittivity.

The pseudo activation energies $E_{a,\sigma i}$ associated with the long-range and interfacial proton conduction mechanisms can be obtained by fitting the values of σ_{EP} and σ_{IP} with the VTF equation.[36] A pseudoactivation energy is derived from a VTF fit and includes both entropy and enthalpy contributions. The pseudoactivation energies $E_{a,\sigma EP}$ and $E_{a,\sigma IP}$ are given as a function of the nanofiller concentration Ψ in Figure 7. The

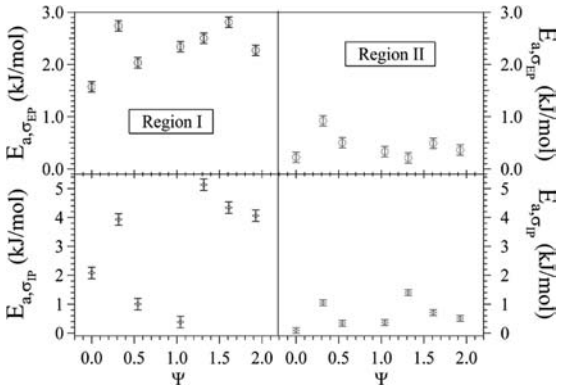

Figure 7. Dependence of the activation energies $E_{a,\sigma EP}$ and $E_{a,\sigma IP}$ on Ψ.

pseudoactivation energies for the conductivity are modulated by the filler in the membrane, but there is no clear trend as a function of Ψ particularly in region I. $E_{a,\sigma EP}$ is higher in the hybrid membranes than in pristine Nafion, and both $E_{a,\sigma EP}$ and $E_{a,\sigma IP}$ are higher in region I than in region II.

These activation energies imply that the segmental motion of the fluorocarbon backbone chains in the PTFE-like domains of Nafion is hindered by the filler in the membrane likely due to the R−SO_3H···[ZrTa] cross-links particularly at lower temperatures in region I where the dynamics of the hydrophobic domains are slower. It is possible to determine the proton diffusion coefficient D_{H+} and the mean distance of proton hopping ⟨r⟩ associated with the bulk conductivity using the Nernst−Einstein (eq 4) and the Einstein−Smoluchowski (eq 5) equations:[23,35,37]

$$D_{H^+} = \frac{\sigma_{EP} RT}{n_{H^+} F^2} \tag{4}$$

$$\langle r \rangle = \sqrt{6 D_{H^+} \tau_{EP}} = \sqrt{\frac{6 \sigma_{EP} \tau_{EP} RT}{n_{H^+} F^2}} \tag{5}$$

where n_{H+} is the charge carrier concentration, R is the universal gas constant, T is the temperature in Kelvin, and F is the Faraday constant. The charge carrier concentration n_{H+} is obtained from the values of PEC[20] and the density of Nafion (1.77 g/cm^3).[34] The values of ⟨r⟩, calculated with eq 5 and shown in Figure 8, are between 40 and 140 nm, increase with

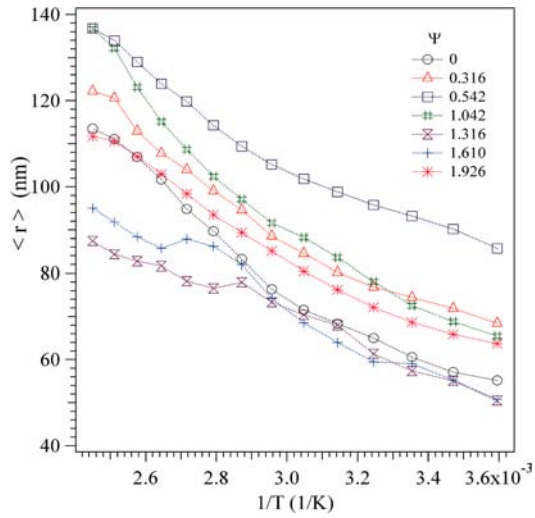

Figure 8. Mean free path of proton hopping ⟨r⟩ as a function of reciprocal temperature.

temperature, and are higher in the hybrid membranes than pristine Nafion. The ZrTa nanofiller facilitates the long-range proton transfer, which occurs via proton exchange processes between different delocalization bodies of the hybrid material where the nanofiller and the dynamic R−SO_3H···[ZrTa] cross-links are solvated by water. A delocalization body (DB) corresponds to the volume of bulk nanocomposite membrane, which contains the nanofiller particles, the hydrophobic domains, and the hydrophilic domains, where the proton in certain pathways can be considered to be delocalized or where the exchange between coordination sites in this volume of bulk membrane, along the considered pathways, is very fast. The concept of a DB can be also generalized to pristine Nafion, where the DB corresponds to a volume of membrane containing only the hydrophobic and hydrophilic domains. Therefore, the long-range migration process occurs when different DBs come into contact due to the dynamics of the host polymer, which are significantly affected by the segmental motion of the hydrophobic domains of the Nafion host matrix. The values of ⟨r⟩ are the mean value of two proton migration distances: inside the DBs (intracluster migration) and between different DBs (intercluster migration), which is the rate-determining step of the long-range charge exchange process.

The results seem to be consistent with the structural model of Nafion proposed by Gebel[38] on the basis of SAXS and SANS studies. The authors claim that Nafion consists of "bundles" of fluorocarbon chains with a diameter of about 4 nm and a length greater than 100 nm, which are surrounded by the electrolyte solution. According to this interpretation, and assuming that the "inter-cluster migration" process is the rate-determining step for the conduction, it is reasonable to hypothesize that long-range charge migration occurs when a proton is exchanged between different DBs. In [Nafion/(ZrTa)$_\Psi$], the DBs are based on bundles of fluorocarbon chains, which are held together by dynamic R−SO_3H···[ZrTa]···HSO_3−R bridges or

dx.doi.org/10.1021/ja3071336 | J. Am. Chem. Soc. 2012, 134, 19099−19107

R−SO_3H···HSO_3−R interacting side groups present within the hydrophilic domains. The results described here reflect a phase-separated geometry and are therefore generally applicable to structural models that incorporate this feature.

4. CONCLUSIONS

This study reports the thermal, mechanical, and electric properties of the [Nafion/$(ZrTa)_\Psi$] membranes. DSC investigations reveal the presence of four endothermic transitions in the 50−300 °C temperature range and demonstrate that the presence of dynamic R−SO_3H···[ZrTa] cross-links increases the thermal stability of the −SO_3H groups and the temperature of thermal relaxation events occurring in hydrophobic domains of Nafion. DMA analysis reveals four mechanical relaxation events: α, α', α_{pc}, and α_{pc}'. The DMA results indicate that the concentration and the strength of the dynamic R−SO_3H···[ZrTa] interactions improve the mechanical stability of both hydrophobic and hydrophilic domains of the hybrid materials. The electrical analysis reveals two electric relaxations associated with the materials' interfacial (σ_{IP}) and bulk proton conductivity (σ_{EP}). σ_{EP} is 2−3 orders of magnitude higher than σ_{IP} and shows VTF behavior, which indicates that the long-range conductivity is closely related to the segmental motion of the Nafion host matrix. The conductivity studies suggest that the concentration and the strength of R−SO_3H···[ZrTa] cross-links significantly affect the conductivity and the stability range of conductivity of the hybrid membranes. The wet [Nafion/$(ZrTa)_\Psi$] membrane with Ψ = 1.042 has a conductivity of 7.0×10^{-2} S cm^{-1} at 115 °C, and a SRC of 5−155 °C. In the same conditions, Nafion shows a conductivity of 3.3×10^{-2} S cm^{-1} and a SRC of 5−105 °C. The results suggest that these new materials are very promising proton conducting systems for application in PEMFCs operating at temperatures higher than 90 °C.

Overall, the results indicate that the ZrTa nanofiller stabilizes both the hydrophobic and the hydrophilic domains of the materials due to the formation of R−SO_3H···[ZrTa]···HSO_3−R bridges, which interconnect the bundles of fluorocarbon chains in a 3D hybrid polymeric network, as shown in Figure 9a and b, which form the delocalization bodies. This produces a reduction in the swelling and an increase in the mechanical properties as compared to Nafion.

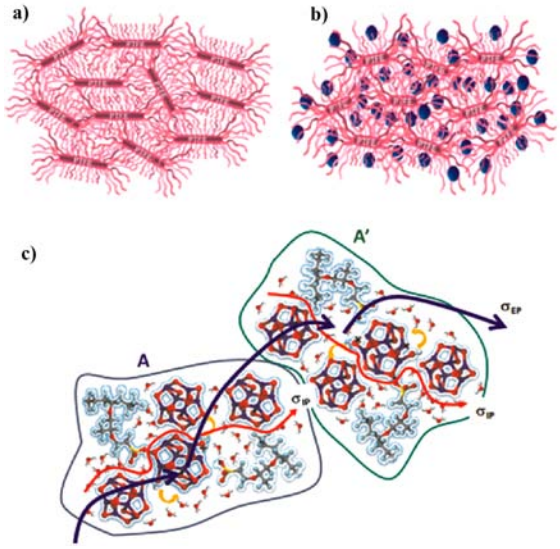

Figure 9. Hypothesized dry membrane structure of pristine Nafion (a) and hybrid membranes (b). (c) Proton conduction mechanism proposed for the wet [Nafion/$(ZrTa)_\Psi$] nanocomposite membranes. A and A′ are two different delocalization bodies (DBs).

Despite a reduction in the water uptake, the [Nafion/$(ZrTa)_\Psi$] membranes have higher bulk and interfacial conductivity values than Nafion. These results suggest that the proton conduction occurs at the interfaces between the Nafion polar domains and the nanofiller, as shown in Figure 9c. The presence of proton percolation pathways at the Nafion−nanofiller interfaces reduces the amount of water necessary to maintain good proton conduction. Long-range conduction (σ_{EP}) occurs when the dynamics of the fluorocarbon matrix induces contact between different DBs, that is, A and A′ in Figure 9c, which results in proton exchange processes between DBs.

AUTHOR INFORMATION

Corresponding Author

vito.dinoto@unipd.it

Present Address

[§]Department of Molecular Science and NanoSystems, University of Venice, Via Dorsoduro 2137, 30123 Venezia (VE), Italy.

Notes

The authors declare no competing financial interest.

ACKNOWLEDGMENTS

This research was funded by the Italian MURST project PRIN2008, entitled "Direct polymer electrolyte membrane fuel cells: synthesis and study in prototype cells of hybrid inorganic−organic membranes and electrode materials", and Regione del Veneto (SMUPR no. 4148, Polo di ricerca del settore fotovoltaico).

REFERENCES

(1) Satyapal, S. *5th International Conference on Polymer Batteries & Fuel Cells*; U.S. Department of Energy, Energy Efficiency & Renewable Energy: Argonne, IL, 2011.

(2) Vielstich, W. In *Handbook of Fuel Cells − Fundamentals, Technology and Applications*; Vielstich, A. L., Gasteiger, H. A. Eds.; John Wiley & Sons: Chichester, 2003; Vol. *1*, p 26.

(3) Laberty-Robert, C.; Valle, K.; Pereira, F.; Sanchez, C. *Chem. Soc. Rev.* **2011**, *40*, 961.

(4) Doyle, M.; Rajendran, G. In *Handbook of Fuel Cells: Fundamentals Technology and Applications*; Vielstich, W., Lamm, A., Gasteiger, H. A., Eds.; John Wiley & Sons: Chichester, 2003; Vol. *3*, p 351.

(5) Grot, W. *Fluorinated Ionomers*; William Andrew: Norwich, NY, 2008.

(6) Iojoiu, C.; Chabert, F.; Marechal, M.; Kissi, N. E.; Guindet, J.; Sanchez, J.-Y. *J. Power Sources* **2006**, *153*, 198.

(7) Sanchez, J.-Y.; Alloin, F.; Iojoiu, C. *J. Fluorine Chem.* **2006**, *127*, 1471.

(8) Alberti, G.; Casciola, M. *Annu. Rev. Mater. Res.* **2003**, *33*, 129.

(9) Aparicio, M.; Klein, L. C. *J. Electrochem. Soc.* **2005**, *152*, A493.

(10) Jalani, N. H.; Dunn, K.; Datta, R. *Electrochim. Acta* **2005**, *51*, 553.

(11) Mauritz, K. A. *Mater. Sci. Eng., C* **1998**, *6*, 121.

(12) Nakao, M.; Yoshitake, M. In *Handbook of Fuel Cells: Fundamentals Technology and Applications*; Vielstich, W., Lamm, A., Gasteiger, H. A., Eds.; John Wiley & Sons: Chichester, 2003; Vol. *4*, p 412.

(13) Neergat, M.; Griedrich, K. A.; Stimming, U. In *Handbook of Fuel Cells: Fundamentals Technology and Applications*; Vielstich, W., Lamm,

A., Gasteiger, H. A., Eds.; John Wiley & Sons: Chichester, 2003; Vol. *4*, p 856.
(14) Satterfield, M. B.; Majsztrik, P. W.; Ota, H.; Benziger, J. B.; Bocarsly, A. B. *J. Polym. Sci., Part B: Polym. Phys.* **2006**, *44*, 2327.
(15) Thampan, T. M.; Jalani, N. H.; Choi, P.; Datta, R. *J. Electrochem. Soc.* **2005**, *152*, A316.
(16) Di Noto, V.; Piga, M.; Lavina, S.; Negro, E.; Yoshida, K.; Ito, R.; Furukawa, T. *Electrochim. Acta* **2010**, *55*, 1431.
(17) Di Noto, V.; Piga, M.; Piga, L.; Polizzi, S.; Negro, E. *J. Power Sources* **2008**, *178*, 561.
(18) Di Noto, V.; Boaretto, N.; Negro, E.; Stallworth, P. E.; Lavina, S.; Giffin, G. A.; Greenbaum, S. G. *Int. J. Hydrogen Energy* **2012**, *37*, 6215.
(19) Di Noto, V.; Boaretto, N.; Negro, E.; Giffin, G. A.; Lavina, S.; Polizzi, S. *Int. J. Hydrogen Energy* **2012**, *37*, 6199.
(20) Di Noto, V.; Piga, M.; Negro, E.; Giffin, G. A.; Polizzi, S.; Zawodzinski, T. A. *ChemSusChem* **2012**, submitted for publication.
(21) Page, K. A.; Cable, K. M.; Moore, R. B. *Macromolecules* **2005**, *38*, 6472.
(22) Carbone, A.; Pedicini, R.; Portale, G.; Longo, A.; D'Ilario, L.; Passalacqua, E. *J. Power Sources* **2006**, *163*, 18.
(23) Di Noto, V.; Piga, M.; Giffin, G. A.; Pace, G. *J. Membr. Sci.* **2012**, *390*−*391*, 58.
(24) Di Noto, V.; Piga, M.; Negro, E.; Giffin, G. A.; Lavina, S. *MRS Online Proc. Libr.***2011**, *1384*.
(25) Di Noto, V.; Gliubizzi, R.; Negro, E.; Pace, G. *J. Phys. Chem. B* **2006**, *110*, 24972.
(26) Rodgers, M. P.; Shi, Z.; Holdcroft, S. *J. Membr. Sci.* **2008**, *325*, 346.
(27) Di Noto, V.; Lavina, S.; Negro, E.; Vittadello, M.; Conti, F.; Piga, M.; Pace, G. *J. Power Sources* **2009**, *187*, 57.
(28) Masetti, G.; Cabassi, F.; Morelli, G.; Zerbi, G. *Macromolecules* **1973**, *6*, 700.
(29) Zerbi, G.; Sacchi, M. *Macromolecules* **1973**, *6*, 692.
(30) Clark, E. S. *Polymer* **1999**, *40*, 4659.
(31) Di Noto, V.; Giffin, G. A.; Vezzù, K.; Piga, M.; Lavina, S. In *Solid State Proton Conductors: Properties and Applications in Fuel Cells*; Knauth, P., Di Vona, M. L., Eds.; Wiley: Chichester, 2012.
(32) Lu, Z.; Polizos, G.; MacDonald, D. D.; Manias, E. *J. Electrochem. Soc.* **2008**, *155*, B163.
(33) *CRC Handbook of Chemistry and Physics*, 86th ed.; Lide, D. R., Ed.; CRC Press: Boca Raton, FL, 2005.
(34) Serghei, A.; Tress, M.; Sangoro, J. R.; Kremer, F. *Phys. Rev. B: Condens. Matter* **2009**, 80.
(35) Kreuer, K. D. *J. Membr. Sci.* **2001**, *185*, 29.
(36) Giffin, G. A.; Piga, M.; Lavina, S.; Navarra, M. A.; D'Epifanio, A.; Scrosati, B.; Di Noto, V. *J. Power Sources* **2011**, *198*, 66.
(37) Atkins, P.; de Paula, J. *Physical Chemistry*, 8th ed.; Oxford University Press: Oxford, 2006.
(38) Rubatat, L.; Rollet, A. L.; Gebel, G.; Diat, O. *Macromolecules* **2002**, *35*, 4050.